



Assessing the efficiency of the irrigation system in a horticulture field through time-lapse electrical resistivity tomography

Agnese Innocenti^{1,2} · Veronica Pazzi^{1,3} · Marco Napoli² · Riccardo Fanti¹ · Simone Orlandini²

Received: 12 July 2023 / Accepted: 4 February 2024
© The Author(s) 2024

Abstract

The characterization by means of geophysical techniques of agricultural soils subjected to continuous irrigation cycles makes it possible to study the heterogeneity of a soil and the preferential pathways of water flows without disturbing soil and plants. A better knowledge of soil heterogeneity enables optimal water resource management in terms of crop, yield, and sustainability. In this study, time-lapse monitoring using electrical resistivity tomographies (ERT) is proposed as a reliable and non-invasive technique to quantify the movement of water flows and thus the variation of soil water content during the irrigation process. ERT surveys have been conducted in melon-growing soils in southern Tuscany (Italy). Five survey campaigns have been carried out between June and August 2022, in which ERT data have been collected by taking measurements before (T_0), during (T_1), and after (T_2) the irrigation phase. The interpretation of the ERT results provided information on the spatial and temporal distribution of water fluxes in the soil and root zone of melons during the irrigation phases. The investigation made it possible to identify the preferential pathways of infiltration of irrigation water, the points where water is absorbed by the roots, and the points where water follows a preferential pathway instead distributing itself entirely below the root growth zone. Thus, this research suggests that the ERT technique can be used to evaluate the efficiency of the irrigation system in order to achieve optimal management of the water resource, avoiding preferential flow paths that lead to less water availability for the plant.

Introduction

Optimizing the irrigation system, increasing its efficiency, and improving freshwater management, is crucial for agriculture in a period of severe climate change. In 2015, the United Nations adopted 17 Sustainable Development Goals (SDGs) to achieve by 2030 a better and more sustainable future for all. Recently, Capello et al. (2021) developed the Geophysical Sustainability Atlas, which facilitates the understanding of the value that geophysics and remote sensing techniques bring to the achievement of each SDG. Specifically, goals numbered 12—Responsible consumption and production, 13—Climate action, and 15—Life on land, point

to the need to reduce water wastage through operational efficiency informed by geophysical monitoring, improving and incentivizing irrigation systems. Geophysical and remote sensing tools/techniques indicated by Capello et al. (2021) to achieve the objectives include: 1. ground-conductivity mapping; 2. resistivity tomography; 3. 3D modelling; 4. satellite remote sensing; 5. UAV imagery; 6. electromagnetic induction surveying; 7. seismic reflection; and 8. gravity.

To date, in agriculture the drip irrigation system, or localized irrigation or micro-irrigation, is considered the most effective method in orchard and horticulture, as it provides significant savings in water, electricity, and offers the possibility of injecting fertilizer during the irrigation phase (Van der Kooij et al. 2013; Ortega-Reig et al. 2017). Although the efficiency of this method is considered high (Brower et al. 1989; Burt et al. 2000; Burton 2010), it can be reduced by certain conditions, such as the soil type (i.e., texture, porosity, structure, and chemical component). Weather conditions, which are increasingly characterized by extreme events such as droughts, heat waves, floods, hailstorms, and long-term rainfall (Arora 2019; Cogato et al. 2019; Malhi et al. 2021; Abbass et al. 2022), can also affect the effectiveness of

✉ Agnese Innocenti
agnese.innocenti@unifi.it

¹ Department of Earth Sciences, University of Florence, 50121 Florence, Italy

² Department of Agriculture, Food, Environment and Forestry, University of Florence, 50144 Florence, Italy

³ Department of Mathematics, Informatics, and Geosciences, University of Trieste, 34128 Trieste, Italy

irrigation. It is therefore essential to achieve high levels of irrigation efficiency to ensure the success of the crop.

Irrigation efficiency is defined as the critical measure of water required to irrigate a field (Howell 2003). It is mainly monitored by measuring the soil volumetric water content (VWC) (Bittelli 2011; Israelsen 1950; Vargas et al. 2021; Yu et al. 2021). VWC expresses the amount of water present in the soil in terms of weight or volume and plays a fundamental role in an agricultural soil, as it is one of the main factors involved in plant growth and nutrition (Jensen 2007; Bittelli 2011). There are multiple techniques commonly used to measure VWC, such as electromagnetic (EM) methods, time domain reflectometry (TDR), and time domain transmission (TDT) (Bogena et al. 2017). Most of the sensors that measure VWC are mainly based on point measurements with a narrow range of investigation both in depth and spatially (Yu et al. 2021, Vargas et al. 2021). For this reason, in recent years geophysical survey techniques have also found wide use in the field of agriculture. In fact, they allow to obtain subsoil volumetric data, with significantly lower costs.

Geophysical techniques are indirect non-destructive investigation methods that allow to reconstruct a subsoil model in terms of layers and materials based on measurements of the physical parameters of the ground. For example, the seismic wave velocities allow to obtain information about the elastic properties, the variation of the gravity at local scale is related to changes in the densities, the electrical (resistivity, conductivity, and chargeability) and magnetic (dielectric permittivity and susceptibility) variations allow to identify different lithologies, water, and waste (Pazzi et al. 2019a, b). Thus, geophysics has various fields of application, including, a) the geological and engineering field to identify the stratigraphy of the subsoil, to search water, to identify buried geological structures, to monitor environmental phenomena like landslides or floods, to detect and track pollutants (Dezert et al. 2019; Pazzi et al. 2019a, b; Di Maio et al. 2020; Hussain et al. 2022; Innocenti et al. 2023); b) the archaeological field for the search of buried anthropic structures (Pazzi et al. 2019a, b; Slepak and Platov 2019; Hannian et al. 2021; Ronchi et al. 2023); and c) the agriculture to support precision farming (Brunet et al. 2010; Garré et al. 2011, 2021; Blanchy et al. 2023; Cabrera et al. 2023).

As reported by Allred et al. (2008), agricultural geophysical investigations are used to characterize the top two meters of soil, which includes the crop root zone, and to investigate soil profiles. Moreover, geophysical surveys make it possible to assess the impact of agricultural practices on the growing season to obtain important information about crop production (Blanchy et al. 2020). The soil can be considered as a resistive–capacitive circuit, where soil properties can influence the resistivity itself (or its inverse called conductivity). The resistivity, in fact, is the capacity of the rock/soil materials to resist the passage of a current and as

a consequence, the conductivity is the rock/soil ability to facilitate the current passage. For example, a soil rich in clay presents lower resistivity (higher conductivity) values than sand or rock, presenting itself as more conductive, just as the presence of salt, which has capacitive behaviour, leads to the identification of a conductive soil (Loke 2014). Thus, Electrical Resistivity Tomography (ERT) is one of the geophysical methods most employed in agriculture (Blanchy et al. 2020). Especially the inverse of resistivity, i.e., the conductivity, has not only found wide use as a proxy in the study of salinity (Callaghan et al. 2017; Brindt et al. 2019; De Carlo et al. 2020), of the water content and soil moisture (Brunet et al. 2010; Beff et al. 2013; Alamry et al. 2017; Vanella et al. 2022) but also of the soil–root interaction (Cassiani et al. 2015; Vanella et al. 2018; Mary et al. 2019) and soil texture (Blanchy et al. 2020). The ERT method estimates the distribution of the electrical resistivity (ER in [Ωm]) of the subsoil by measuring the electrical potential difference at different points on the ground surface. From ER data, electrical conductivity (EC in [S/m]) values can be easily obtained as $1/\text{ER}$. Resistivity/conductivity is linked to various parameters such as: texture, skeleton, salinity, porosity, mineral and fluid content, and degree of water saturation in the soil (Allred et al. 2008; Loke 2014).

In recent years, ERT has been applied with good results to the study and monitoring of irrigation systems in agriculture. For example, Vanella et al. (2022) used electrical tomography to monitor soil water flow in a micro-irrigated orange grove and found the importance of geophysical techniques such as ERT in aiding irrigation system management, particularly in estimating the amount of water needed for irrigation to reduce wastage. Acosta et al. (2022) used ER measurements to model water content along the soil profile showing that the ERT technique can be a useful tool to estimate soil moisture, to represent moisture zones in the soil profile, and to estimate the water stress coefficient. Vargas et al. (2021) applied electrical tomography to detect irrigation uniformity and deep infiltration during irrigation demonstrating that there is a relationship between ERT data and VWC in a soil under irrigation and that ERT images have been able to show preferential pathways in the distribution of moisture at depth.

The main research question of this study concerns the actual efficiency of the two-drip-wing system employed in a field used for growing melons. This kind of irrigation system is usually installed in the upper portion of the mulch ridge (where the melon plants grow) with the two-drip-wing positioned on the top portion of a mulch ridge, therefore laterally and a few centimetres away from the melon plants. The study was carried out to evaluate its efficiency in distributing the water to ensure that all the roots are reached and that the soil is kept above the capacity of the field. The analysis was carried out

employing the ERTs as a reliable and non-invasive technique in this kind of agricultural application. It is indeed essential to know the distribution pattern of irrigation water in the subsoil and root zone to plan the optimal irrigation system according to the crop and field conditions and to schedule the irrigation phases.

ERT investigations have provided important insights to describe the soil structure, to identify the accumulation of irrigation water under the root zone by exploiting the sensitivity of ER to VWC variation. Therefore, the objectives of this work are: 1) to define the degree of uniformity of irrigation water distribution by means of the ERT technique capability of identifying soil structure and areas of water accumulation, 2) to identify the presence of preferential pathways in irrigation water flows within the ridge of the plastic mulch film, and thus 3) to evaluate the efficiency of the two-drip-wing system on a mulch ridge in a melon cultivated field.

The test site is described in Sect. "Study site", while Sect. "Methods" presents details about the employed methodology. The results of the ERT monitoring and the discussions of the three above-mentioned work objectives are presented in Sect. "Results" and Sect. "Discussion", respectively.

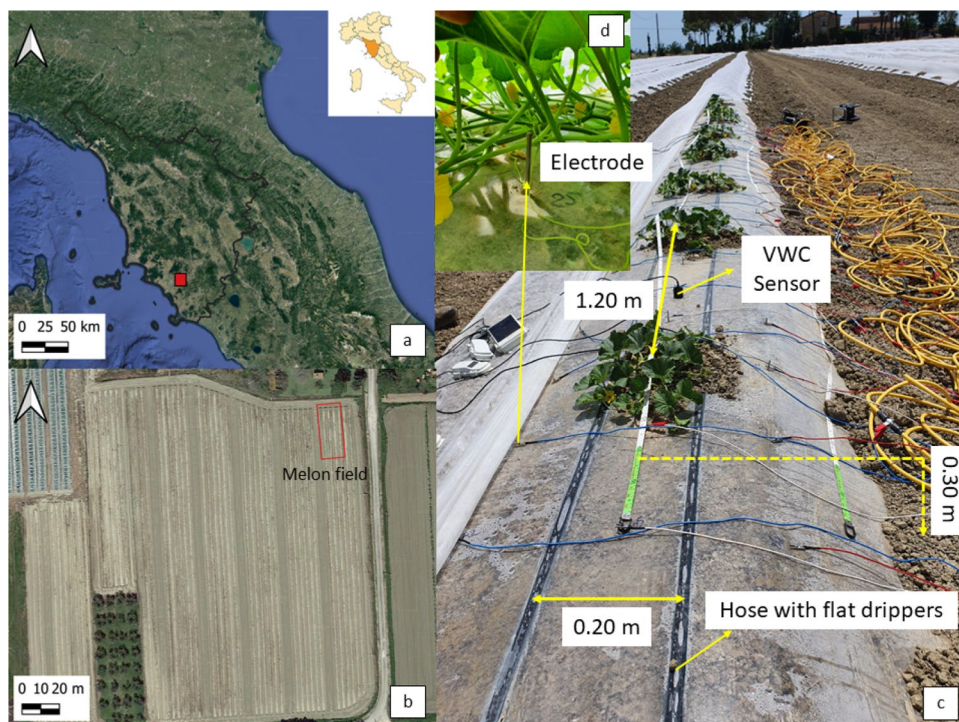
Study site

The study has been conducted in an agricultural field used for the cultivation of melons (*Cucumis melo*) at Barbaruta (42.804113°N, 11.02322°E; 19 m a.s.l.) in the municipality of Braccagni (Grosseto, Tuscany—Italy) (Fig. 1). The survey site is characterized by sodium-rich soils. In detail, these are irrigated plots of land where sodium accumulation has occurred over time. These soils, derived from land reclamation, must be maintained above the irrigation capacity of the field to keep crops in good condition.

The area (southern Tuscany) is characterised by a climate mitigated by the proximity of the sea and it has hot summers, constantly ventilated by the sea breeze from the West, and winters that are not particularly cold. Average annual temperatures are around 15 °C in the lowland areas, with average values around 8 °C in January and close to 24 °C in July. Rainfall, which is rather limited and concentrated mainly in the autumn period, is generally of short duration, sometimes in the form of thunderstorms (Fig. 2). On average, they fluctuate around 600 mm per year.

In this study, the melon plants are oriented North–South and positioned above a 30 cm high ridge. The space between one plant and the next is 1.20 m (Fig. 1c). The field is irrigated using a two-drip-wing system, positioned at the highest part of the ridge, approximately 20 cm apart (Fig. 1c). The drippers are 60 cm apart and have a flow rate of 1 l/h.

Fig. 1 **a** Location of the study area near Grosseto (Tuscany, Italy); **b** red rectangles indicate the melon field object of the present study; **c** photo of the ERT profile detail along a row of melons; **d** zoom of one electrode



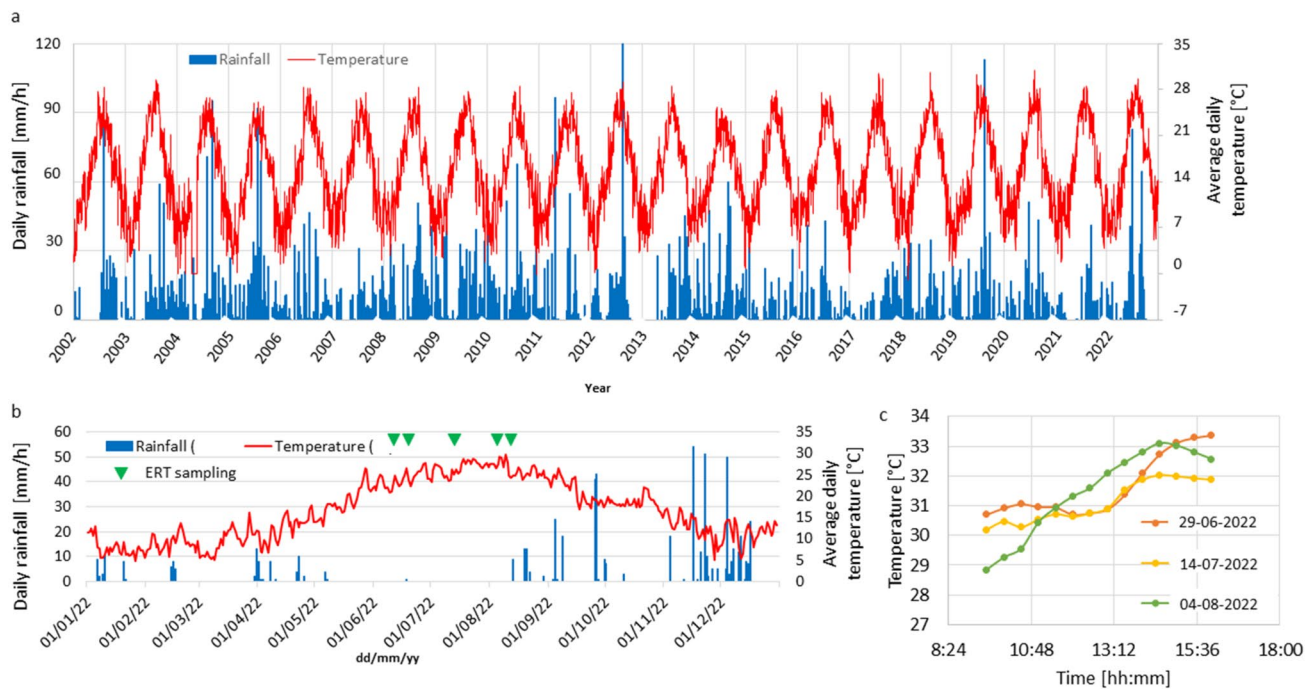


Fig. 2 **a** Graph of daily rainfall and average daily temperature for the last 20 years (2002–2022); **b** Rainfall intensity and temperature between January, 1st 2022 and December, 31st 2022. The graph shows for June, July, and August 2022 (the period when the surveys have been carried out) an almost total absence of precipitation. Data have been retrieved by <http://www.sir.toscana.it/consistenza-rete>.

During the study, irrigation occurred every 3 days for 3.5 h/day, releasing into the soil 25 ml per m^3 (Fig. 1c).

Methods

The time-lapse ERT setup and the VWC monitoring system

ERT is an active geophysical method that provides 2D or 3D images of the distribution of ER in the subsurface. These images show the variations in resistivity due to the nature of the soils, their structure, and degree of saturation (Perrone et al. 2014; Pazzi et al. 2018; Patrizi et al. 2022).

The method consists of inducing an electric current in the ground by means of a pair of electrodes, called current electrodes, and determining the distribution of the induced electric potential field by means of another pair of electrodes, called potential electrodes. Thus, electrodes placed in the ground at a certain distance are used both to induce current (I) into the ground and to determine the voltage measurement (V). Knowing the values of I and V and the geometric coefficient (k), which depends on the electrode configuration adopted (i.e., the four electrodes employed to measure I and V), the apparent resistivity value can be calculated (Patrizi

et al. 2022). The purpose of ERT investigations is to determine the distribution of subsurface resistivity from measurements of apparent ground resistivity (ρ_a). The apparent resistivity value (ρ_a) is defined using the following formula (Dahlin and Zhou 2004; Loke 2014; Perrone et al. 2014; Pazzi et al. 2019a, b):

$$\rho_a = k \frac{\Delta V}{I} [\Omega m] \quad (1)$$

However, ρ_a does not represent the true resistivity of the soil but each measure is a sort of mean resistivity value of a homogeneous subsoil from the top up to the depth of investigation. Thus, to obtain the distribution of the real soil resistivity, an inversion process of ρ_a data must be carried out, and this is done using known algorithms (Santarato et al. 2011; Loke 2014).

Electrical resistivity (ER) is expressed by the Greek letter (ρ) and is measured in [Ωm]. Electrical conductivity (EC), on the other hand, is represented by the Greek letter σ and, as already said in the Introduction, it is defined as the inverse of resistivity and the unit is [S/m]. Thus, high resistivity values are equal to low conductivity, and vice versa (Heaney 2003).

The ERT measurements have been carried out by creating a 3D grid in which the 72 electrodes have been spaced 0.3 m apart and arranged in 3 parallel lines, 0.3 m apart

and 6.9 m long for a total of 24 electrodes per line (Fig. 3). The electrode set up has been chosen after some test in the same field with different electrode configuration layouts (not shown here for brevity). The configuration It allowed 6 melon plants to be incorporated into the ERT grid (Innocenti et al. 2022). The central electrode line (electrodes 25–48) has been positioned in the centre of two-drip-wing, while the other two lines (electrodes 1–24 and electrodes 49–72) have been positioned outside the irrigation system (Fig. 3).

The high-resolution 3D ERT measurements have been conducted in 5 campaigns at regular intervals between June and August 2022, applying the Time-Lapse technique (Ma et al. 2011; Calamita et al. 2012; Blanchy et al. 2020), i.e., taking measurements at different times during the period of interest, in this case collecting data before (T_0), during (T_1), and after (T_2) the irrigation phase. This technique made it possible to investigate the behaviour of the soil over time during the various irrigation phases and during the growth phase of the crop. During the first campaign on June, 16th 2022, the chosen electrode set up, has been installed so that they could remain embedded in the ground for the duration of the surveys, thus avoiding changing the position and depth of the electrodes. The set consists of 72 stainless-steel (304) electrodes with a length of 15 cm and a diameter of 5 mm. During the campaign of June, 16th 2022, data were acquired for times T_0 and T_1 . During the campaigns of June, 29th 2022, July, 14th 2022, and August, 4th 2022, resistivity values were recorded for times T_0 , T_1 , and T_2 . While the last campaign (August, 25th 2022) only included measurement acquisition for time T_0 , as irrigation is no longer performed during the harvest phase. Considering the main objective of the work, i.e., to show the variation of EC during the irrigation phase, only those measurements that recorded all three times are shown in this work (June, 29th 2022, July, 14th 2022, and August, 4th 2022).

The data acquisition has been performed with a 10 channel Syscal Pro georesistivimeter (Iris Instruments, France) and the use of the above-mentioned stainless-steel electrodes connected by multiple cables. The input voltage was of 800 V, the number of readings for each energisation (i.e., the stack range) was set from a minimum of 2 to a maximum of 5, and the quality factor q (i.e., the parameter to decide

how many readings perform at each step) was of 2%. A total of 4950 recorded data for each dataset have been collected using a Dipole–Dipole electrode configuration (Dahlin and Zhou 2004; Loke 2014; Pazzi et al. 2019a, b; Catelani et al. 2021) (Table 1). The acquisition of each dataset required about 2 h. In the optimal condition, the adopted array allows for a survey depth of approximately 1.15 m well beyond the target depth (i.e., the plants' roots depth that is about 0.30–0.40 m). This depth could be reduced of a 20–30% if the soil is too conductive because the current remains trapped in the conductive layer, but the target is still well included. The commercial software ViewLab 3D (Geostudi Astier S.r.l., Multi-Phase Technologies LLC) has been used to pre-process and to invert the geoelectrical data (Bellanova et al. 2020; Sendrós et al. 2020; Balasco et al. 2022). The software makes it possible to remove outliers, to increase the quality of the measurements and to calculate the frequency distribution of voltage, current intensity, geometric factor, and apparent resistivity distribution by statistically analysing the dataset, going on to eliminate the extremes of the tails of each distribution. It enables optimal data management by implementing Occam's regularisation (Santarato et al. 2011; Binley 2015; Viero et al. 2015; Pazzi et al. 2018).

Table 1 ERT name, electrode distance, total number of measurements acquired, number of data removed, and total number of iterations required to obtain the convergence (i.e., reach a residual value lower than the misfit function between the field and the modelled data) of the inversion procedure

Name	Electrode spacing [m]	Acquired data [adim]	Removed data	Iteration number [adim]
T_0 29-06-2022	0.3	4950	69 (1.4%)	3
T_1 29-06-2022	0.3	4950	107 (2.2%)	7
T_2 29-06-2022	0.3	4950	74 (2.9%)	7
T_0 14-07-2022	0.3	4950	144 (2%)	7
T_1 14-07-2022	0.3	4950	108 (1.7%)	9
T_2 14-07-2022	0.3	4950	98 (2%)	7
T_0 04-08-2022	0.3	4950	82 (1.7%)	7
T_1 04-08-2022	0.3	4950	102 (2.1%)	7
T_2 04-08-2022	0.3	4950	103 (2.1%)	8

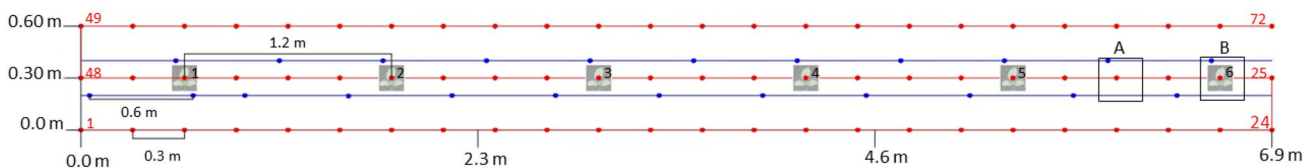


Fig. 3 **a** Electrode set up arranged in five parallel lines with the inclusion of two plants; **b** Electrode set up arranged on 3 parallel lines with the inclusion of six plants. In both **a** and **b** the red dots represent the electrodes marked by red numbers and the blue dots represent the

drip tube. The rectangles marked as A and B represent the placement of one 10HS probe midway between the fifth and sixth plants (A) and the second probe placed near the sixth plant

In addition, the software made it possible to create a mesh of square cells with a side of 0.15 cm, equal to half the distance between the electrodes. For each dataset a mesh of 37,260 ($69 \times 27 \times 20$) nodes were generated and employed in the inversion procedure. The data from each campaign were inverted individually using the same mesh for all of them and a starting model of homogeneous resistivity of 6 Ωm . This initial value was chosen as the average of the 15 average apparent resistivity values of each dataset retrieved from the histogram distribution (Viero et al. 2015). It represents, in fact, the necessary value to be assigned to the starting homogeneous half-space. All inversion ERTs were carried out with a noise value (i.e., the error that affect field data) of 5% and achieved convergence, i.e., the resistivity models have a residual value lower than the misfit function between the field and the modelled data (Santarato et al. 2011). For each dataset in Table 1 are summarized the number of removed data because considered outliers and the iterations required to reach the convergence of the model.

The VWC has been acquired on the North portion of the 3D ERT grid by installing two HOBOnet Soil Moisture 10HS sensors connected to a HOBOnet datalogger that records soil moisture every 30 min (A and B in Fig. 3). The moisture sensor complements the ECH2O™ 10HS sensor and provides readings directly in VWC. The probes having a length of 15 cm, have been installed vertically in the soil, allowing the measurement of soil moisture of 0.001 m³ volume of soil, with a survey depth of 15 cm. The sensors were checked to ensure that the measured data corresponded to the water value in the soil.

The HOBOnet MX2300 Series Temp sensor was installed close to the moisture sensor located in A (Fig. 3). It recorded the soil temperature at a depth of 20 cm. As shown in Fig. 2c the soil temperature variation recorded is similar for all the three ERT campaign and a maximum variation of 4 °C in the first 20 cm depth was measured. It is known that the resistivity can not only be influenced by the temperature (Hayley et al. 2007; Jodry et al. 2019) but as also reported by some authors (e.g., Nijland et al. 2010) that a soil temperature variation of few degrees results in neglectable resistivity variations compared to those induced by the soil moisture variations. Therefore, in the following analysis of ERT data no corrections to take into account the soil temperature variation was performed.

The comparison between EC and VWC, and the time-lapse monitoring

The results of the ERTs have been evaluated in the context of the irrigation cycle by correlating the resistivity and/or conductivity values with the VWC recorded by the probes positioned near the sixth plant included in the ERT grid and in the middle between plant number 5 and 6 (see Fig. 3 for

the plants location). To estimate the relationship between ER, or its inverse the EC, and soil moisture, VWC data recorded by the Hobo 10HS probe have been correlated with ER and EC data. Since the probe records an averaged value of VWC over a depth range of 15 cm, the ER and/or EC data have been obtained by averaging the resistivity model values in the first 15 cm in the volume around the probes (A and B in Fig. 3). The average VWC has been calculated as the arithmetic mean among the VWC data collected every 30 min during the ERT acquisition.

To better highlight the spatio-temporal EC variation from the ERT data, the EC percentage changes for each cell (or node) of the mesh that represent the investigated volume were calculated according to the following equation:

$$EC = \frac{(T_i - T_0)}{T_0} \cdot 100 \quad [\%] \quad (2)$$

where EC [%] is the EC variation normalized with respect to the T_0 values, T_i are the EC values of the inverted model during or after irrigation (T_1 and T_2 in this case) and T_0 are the EC values of the inverted model at the initial condition (in this work it coincides with the time T_0 , before irrigation). These obtained EC [%] values are then shown as vertical slices, in the same ways as ERTs.

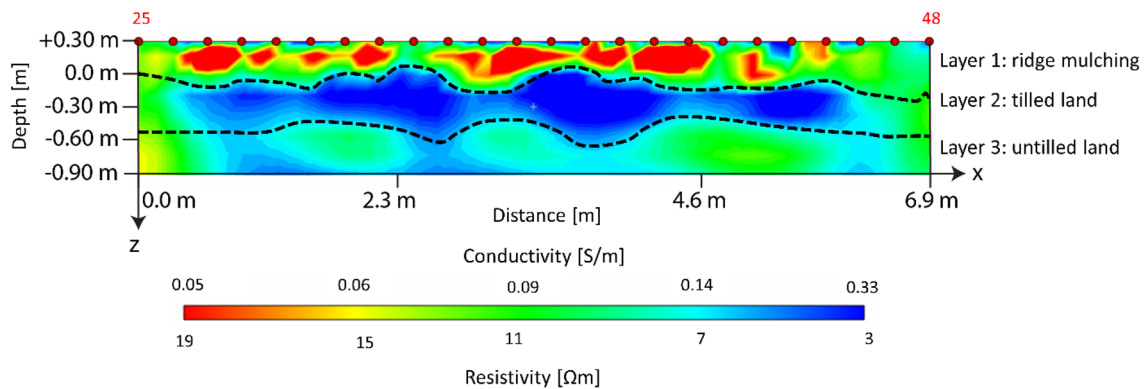
Results

The survey campaigns included the acquisition of 3 ERT measurements for all 5 campaigns, for a total of 15 high-resolution 3D ERT profiles. However, due to logistical problems, only 12 3D ERT can be utilised and the only three campaigns (per month, i.e., June, 29th 2022, July, 14th 2022, and August, 4th 2022; see Table 2) have pre (T_0), during (T_1), and post (T_2) irrigation measurements. The results of all ERTs are concurrent in showing a layered structure made of 3 layers. Figure 4 shows an example of the subsoil stratigraphy identified by resistivity changes in the soil. The first layer (Layer 1 in Fig. 4), the superficial one, is in the range of about +0.30–0.00 m and represents the soil of the mulch fill. It is characterized by an extremely tilled silty clay soil and consequently has pores of a size to retain irrigation water. The roots of the melon plants are in this soil layer. The second layer (Layer 2 in Fig. 4) is identified at the depth between about 0.00 m (ground level) and –0.40 m, the maximum depth reached during tillage by plow. It is an extremely impermeable layer in which water accumulation occurs over time. Finally, the third layer (Layer 3 in Fig. 4) identified is in the depth range of about –0.40 to –0.80 m (depth reached by geoelectric measurements).

The resistivity variations have been evaluated by observing the resistivity distribution before (T_0), during (T_1), and

Table 2 Range of resistivity values of each identified layer for each acquisition campaign

Date	Layer	T_0 —Pre-irrigation	T_1 —During irrigation	T_2 —After irrigation
06/16/2022	Layer 1	7–15 Ωm	3–17 Ωm	/
	Layer 2	5–11 Ωm	3–11 Ωm	/
	Layer 3	7–11 Ωm	7–11 Ωm	/
06/29/2022	Layer 1	5–19 Ωm	3–15 Ωm	3–19 Ωm
	Layer 2	3–7 Ωm	3–5 Ωm	3–5 Ωm
	Layer 3	3–5 Ωm	3–7 Ωm	3–7 Ωm
07/14/2022	Layer 1	11–19 Ωm	7–19 Ωm	5–19 Ωm
	Layer 2	3–7 Ωm	3–7 Ωm	3–5 Ωm
	Layer 3	3–5 Ωm	7–11 Ωm	7–11 Ωm
08/04/2022	Layer 1	15–19 Ωm	5–19 Ωm	5–19 Ωm
	Layer 2	3–5 Ωm	3–5 Ωm	3–7 Ωm
	Layer 3	7–15 Ωm	11–19 Ωm	7–11 Ωm
08/25/2022	Layer 1	15–19 Ωm	/	/
	Layer 2	3–5 Ωm	/	/
	Layer 3	3–7 Ωm	/	/

**Fig. 4** Example of soil stratification detected by ERT. The section corresponds to the acquisition of July 14th, 2022 at time T_2 (during irrigation) and is related to the central line of electrodes (25–48 in Fig. 3)

after (T_2) the irrigation for each single campaign, i.e., during the growth phase of the crop, and subsequently the variation over time considering the entire duration of the cultivation and irrigation phase. Table 2 shows the resistivity values observed over time during each campaign. It is possible to observe that layer 2 has lower resistivity values on average than layer 1, and these values tend to decrease during the irrigation phase. The same phenomenon is observed in layer 3, which, however, presents slightly higher resistivity values than layer 2. This could be caused by the presence of an impermeable layer in which an accumulation of water occurs over time and which the electrical tomography identified as layer 2, and that is the responsible for the decrease in the total depth reached by the survey.

Figure 5 shows the values of the VWC related to the two soil moisture sensors (A and B in Fig. 3) for the whole monitoring period. The peaks on the graph represent the various irrigations carried out. Because of a probe malfunction, data

for the period between June, 30th 2022 and July, 9th 2022 are missing. Looking at the graph, the irrigation peaks show a constant trend over time, just indicating that these peaks are due to irrigation water, also confirming the absence of precipitation that occurred during the study period (Fig. 2). It also denotes a detachment of the VWC curve recorded by the probe located in the middle between two plants (orange curve in Fig. 5) compared to the data recorded by the probe near the plant (blue curve in Fig. 5). This could be caused by the roots retaining water by keeping the soil wetter in the surroundings, showing a higher VWC value than the probe located between two plants (orange curve in Fig. 5).

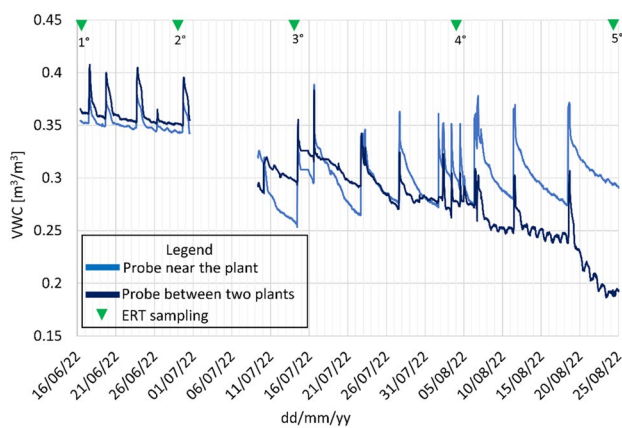


Fig. 5 Temporal variation of soil volume water content (VWC) measured by Hobo sensors installed in the study area. Blue light curve represents data acquired near plant 6 (see Fig. 2 for the location) while blue dark line represents data acquired in the midpoint between plant 5 and 6 (see Fig. 2 for the location). Data between June, 30th 2022 and July, 9th 2022 are missing because of technical problems in the acquisition system. Green triangles indicate the date of the ERT campaigns, only 2°, 3°, and 4° are presented in this work

Discussion

Relationship between ER (or EC) and soil moisture

Figure 6 shows the relationship between the average VWC and the ER and/or EC for each campaign and for each phase. Triangle, square, and dot symbols represent the acquisition time before (T_0), during (T_1), and after

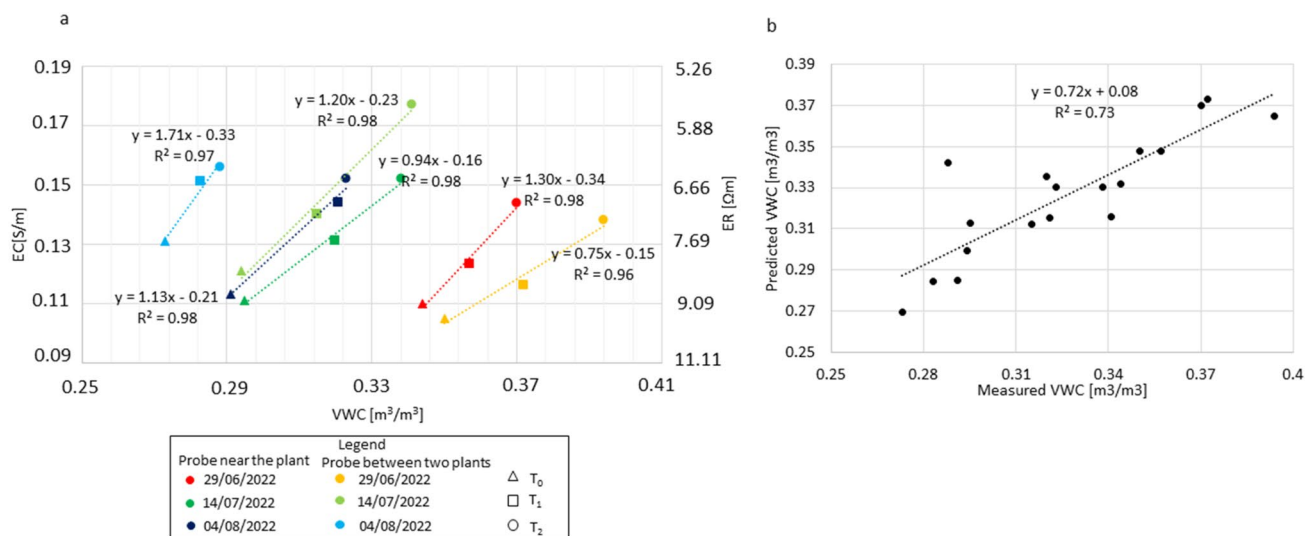


Fig. 6 **a** Relationship between the average VWC, EC and ER. Triangles compare the value of ER/EC and VWC at time T_0 (before irrigation), squares at time T_1 (during irrigation), and dots at time T_2 (after irrigation). Dark colours (red, green, and blue) represent the three

irrigation (T_2), respectively. The colours, on the other hand, represent the different campaigns with respect to the probes position close to a plant (dark colours) and in the middle between two adjacent plants (light colours). Data are also summarized in Table 3. As it is well known, the electrical EC is directly proportional to the VWC; in fact, as the water content increases, the ER decreases. It is clearly visible in Fig. 6 where for each campaign EC and VWC increase during the irrigation phase (i.e., for each colour moving from the triangle to the dot passing for the square). Looking at the data over time, we observe that the initial VWC decreases during the campaigns, i.e., from June (red/orange values) to August (dark and light blue), as the soil is drier. These results agree with that of Vargas et al. (2021), where a direct proportionality between EC and soil moisture is shown.

Values in Fig. 6 show that a linear correlation between EC and VWC exist and that all the regression lines have a similar slope. The average slope of these lines was calculated to be 1.17 with a standard deviation of 0.33. Given a soil volume (e.g., the one investigated by the ERT) changes in conductivity can be attributed either to changes in water content or to changes in the physical characteristics of the soil, such as an increase or decrease in salinity. The conductivity of the irrigation water was measured with HANNA handheld conductivity meter sensor model HI 99310, directly measuring the well water used for irrigation. It was equal to 0.14 S/m, a value in agreement with the conductivity values measured by electrical tomography. Therefore, it is possible to assess with a certain degree of confidence that the changes in EC are primarily due to moisture changes as

campaigns for the probe near the plant, while light colour (orange, light green, and light blue) those for the probe placed between two adjacent plants. **b** Measured VWC versus predicted VWC using ANCOVA calibration model

Table 3 Values of ER and EC calculated in A and B (see Fig. 3 for the location), and the average VWC recorded by Hobo probes

Date	Sensor near the plant number 6			Sensor between plant number 5 and 6		
	ER	EC	VWC	ER	EC	VWC
T_0 29-06-2022	9.073	0.11	0.344	9.55	0.105	0.35
T_1 29-06-2022	8.127	0.123	0.357	8.612	0.116	0.372
T_2 29-06-2022	6.952	0.144	0.37	7.257	0.138	0.394
T_0 14-07-2022	9.02	0.111	0.295	8.261	0.121	0.294
T_1 14-07-2022	7.645	0.131	0.32	7.138	0.14	0.315
T_2 14-07-2022	6.561	0.152	0.338	5.66	0.177	0.341
T_0 04-08-2022	8.84	0.113	0.291	7.626	0.131	0.273
T_1 04-08-2022	6.933	0.144	0.321	6.604	0.151	0.283
T_2 04-08-2022	6.562	0.152	0.323	6.418	0.156	0.288

conductivity in the root zone increases following the irrigation event. Therefore, this linear relationship could describe the relationship between EC and VWC in this type of soil, which is particularly rich in clay and subject to frequent irrigation cycles during melon cultivation. Therefore, it is hypothesised that this linear correlation can be extended to the whole ERT profile and can be used as a proxy for estimating changes in water content given a variation in the EC along the whole ERT profile. That is, having an initial ERT measurement and several measurements taken during the irrigation cycles, it is possible to quantify the relative variations of VWC in the whole portion of field investigated by the ERT. Moreover, having a point VWC it is also possible to individuate the absolute VWC variation between two different time T_i and T_j .

The linear relationship shown in Fig. 6a was quantified by conducting an analysis of covariance model (ANOCOVA) (Corwin and Lesch 2014), whereby the effect of the EC covariate on the VWC value was assessed with categorical independent variables time (T_0 , T_1 , T_2) and location (near plant, between plants). The graph in Fig. 6b shows the results measured VWC values (x -axis) and predicted VWC values (y -axis) from EC data estimated using the ANOCOVA model. The analysis shows that the slope is significant at 1%, as it must be greater than or equal to 0.708 to be significant, and the R^2 value obtained is 0.73. The slope is therefore significant and the model underestimates the data by 3%.

For each campaign, the ERT results of the three phases of the irrigation cycle have been correlated with the corresponding VWC curves (Fig. 7a–c for June, July, and August, respectively). The graphs on right show the VWC curves of the two probes (blue curve near plant 6, orange curve between plants 5 and 6; see Fig. 2 for their location), while the squares and triangles correspond to the EC calculated from the ERT models (shown on left) in the volumes indicated as A and B for each acquisition time (A corresponds to the area of the probe placed between plants 5 and 6, B to the area of the probe placed near the plant number 6). Once

again, it is clearly visible how the EC values trend agrees with that of the water content curve, showing an increase in EC as water content increases. Because of the long duration (about 2 h) of the ERT caused by the high number of acquisitions (see Sect. "Methods" for more details), while the EC value is representative of the VWC before and after the irrigation, i.e., when the irrigation system is turned off, it cannot be used as indicator during the irrigation phase. An attempt to try to use EC as indicator of the VWC variation during the irrigation phase could be carried out reducing the ERT acquisition duration. This could be achieved only avoiding any increment of the distances " a " (distance between the electrodes, see Catelani et al. 2021; Patrizi et al. 2022) and " n " (distance between the last current electrode and the first voltage electrode, see Catelani et al. 2021; Patrizi et al. 2022) in the acquisition sequence, but it will result in a decreasing of the spatial resolution of the ERT. Thus, further analyses are needed to evaluate the effectiveness of speed up the time acquisition losing resolution as a cost-effective way to spatially monitor the VWC during the irrigation phase.

Time-lapse resistivity (or conductivity) monitoring

Looking at the results as a function of irrigation time, in layer 1 it is evident a decrease in resistivity in the transition from the pre-irrigation phase (T_0) to the post-irrigation phase (T_2). Observing the sections shown in Fig. 8, an increase in EC is observed in the surface portion of the ridge (first 10 cm of soil) during irrigation and in the post-irrigation phase. This increase is observed at the drippers and in the post measurements it is noted how the infiltration water penetrates more in some points along the profile than in others. The portions with higher resistivity present in the first 30 cm are cut by the infiltration of water and in the post-irrigation measurements the preferential paths of the water along the profile of the ridge are well denoted, highlighted in Figs. 8, 9, and 10 by dashed white lines.

As far as layer 2 is concerned, the values listed in the Table 2 show a decrease in resistivity passing from the

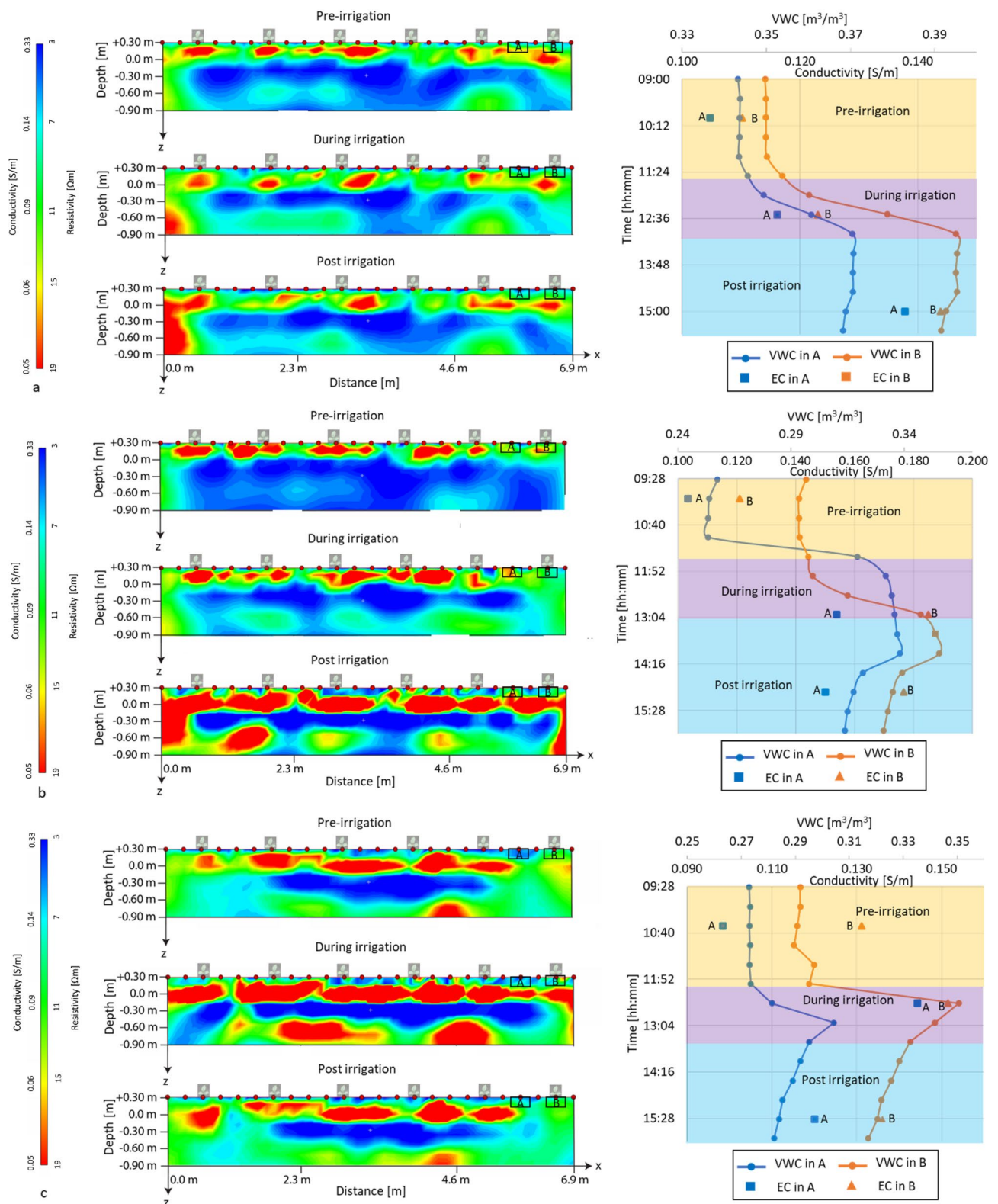


Fig. 7 Comparison of electrical tomography results with VWC. The left panels show the EC sections acquired at the middle row of electrodes (0.30 m). Rectangles A and B indicate the locations of the two moisture probes. The right panels, on the other hand, show the curves of VWC variation over time. The blue rectangles labelled A and the

orange triangles labelled B represent the EC values over time. **a** EC-VWC comparison for the measurement acquired on 29th, June 2022; **b** EC-VWC comparison for the measurement acquired on 14th, July 2022 and **c** EC-VWC comparison for the measurement acquired on 4th, August 2022

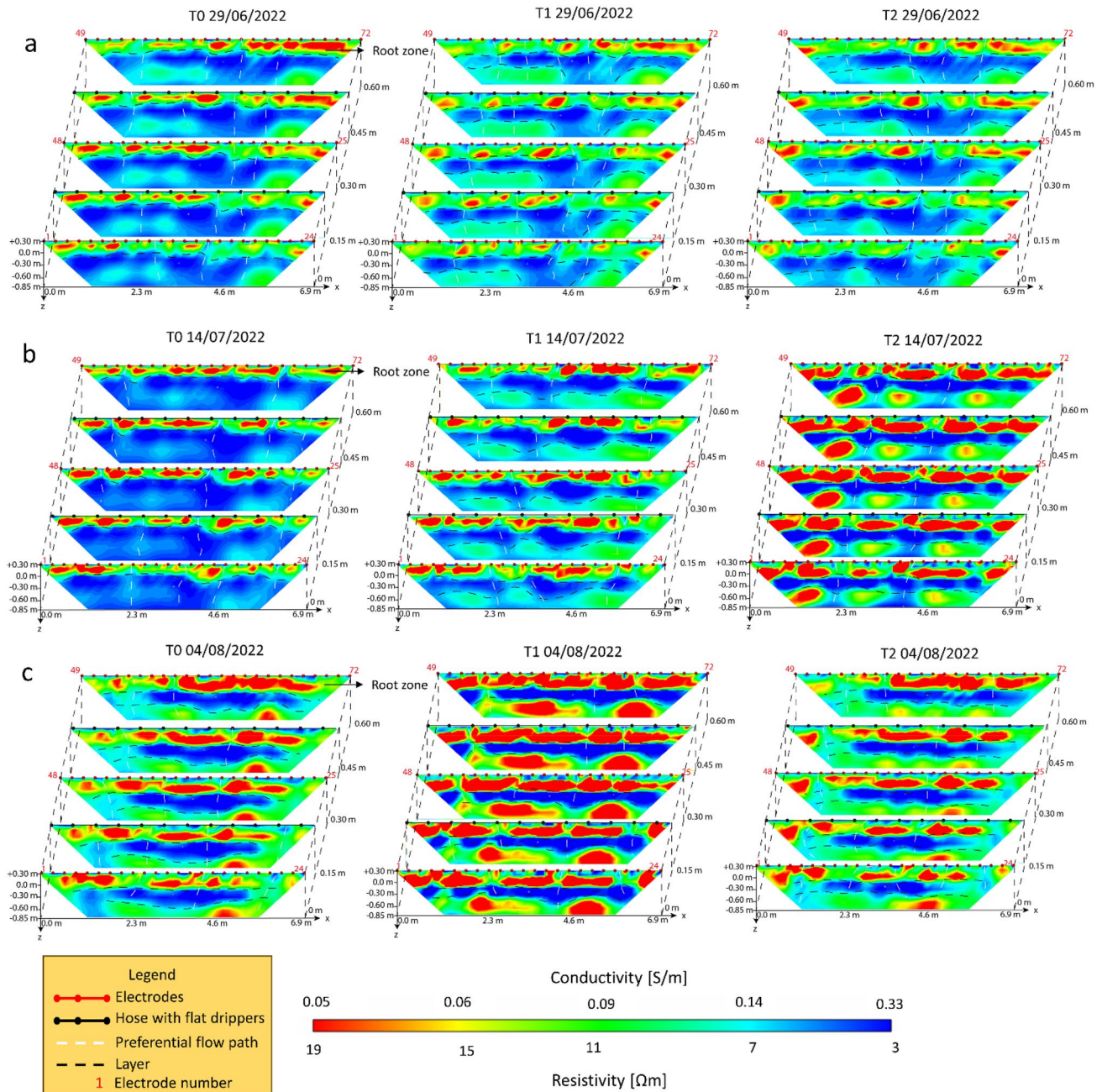


Fig. 8 a ERTs campaign results of June, 29th 2022; **b** ERTs campaign results of July, 14th 2022; ERTs campaign results of August, 4th 2022. The black lines represent the layers, while the white lines

represent the preferential paths of the flow lines. The y scale has been exaggerated to allow the visualization of more sections

pre-irrigation phase (T_0) to the post-irrigation phase (T_2). The decrease in EC in some areas of layer 2, at time T_1 and T_2 , can be attributed to an artefact due to the simultaneous inflow of current and water. On the other hand, observing Fig. 8, this layer becomes more and more conductive during irrigation. In fact, it represents a particularly impermeable layer in which the water tends to concentrate more. Layer 3 is the one that undergoes the greatest variation in resistivity.

In fact, a decrease in resistivity is not always observed during the irrigation phase, but in some cases this area appears to have an increase in resistivity in some areas.

In observing data individually there is generally a decrease in resistivity during and after the irrigation phase, while observing data over the time it can be seen that the soil is more conductive in the initial phase (June 2022) compared to the measurements performed

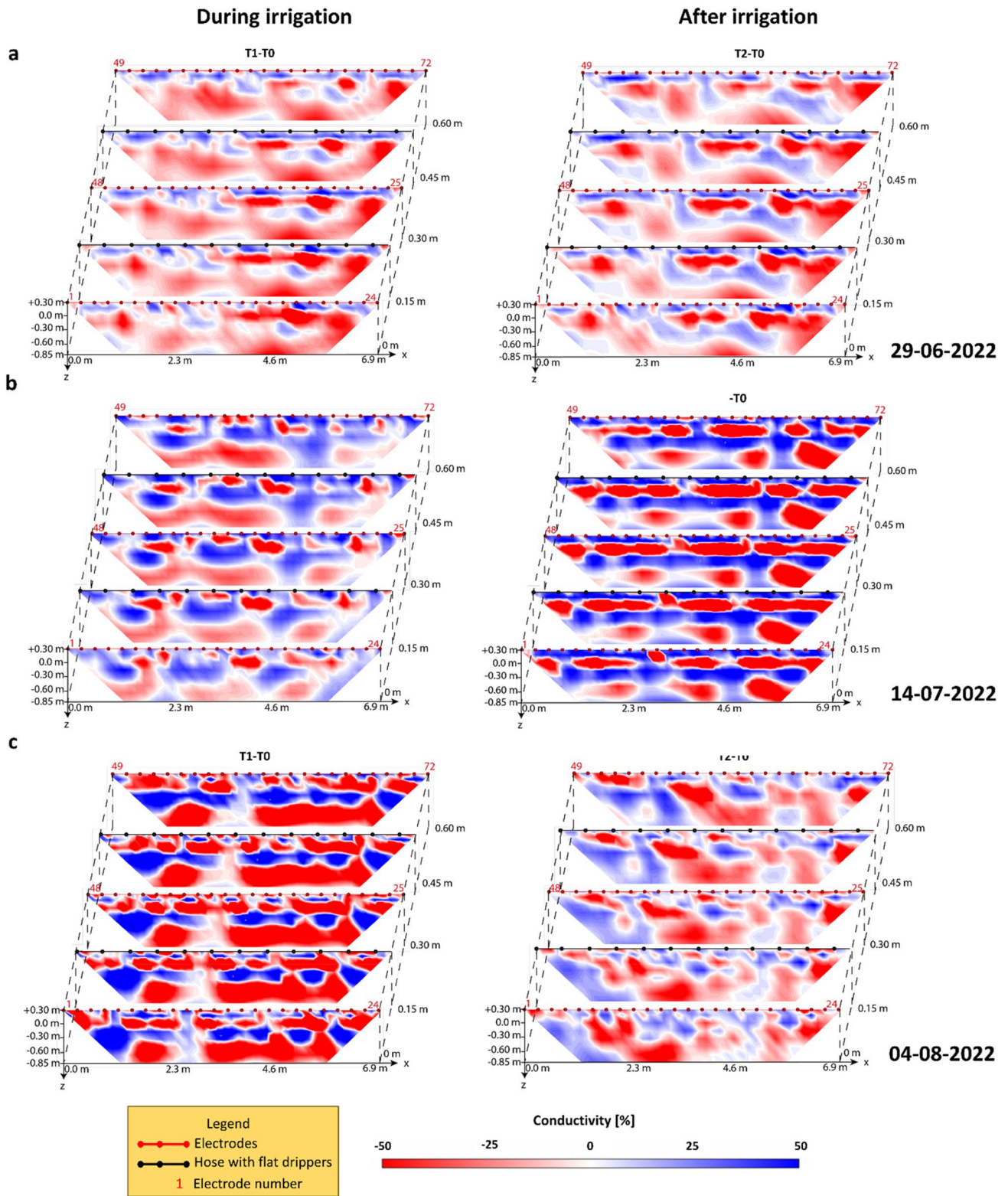


Fig. 9 EC changes (%) observed during T_1 and T_2 times. Panel **a** reports the conductivity tomographies relating to the measurements carried out on 29 June 2022, **b** 14 July 2022 and **c** 4 August 2022. The images relating to during irrigation show the variation in conduc-

tivity between the times T_0 and T_1 , while those relating to after irrigation at times T_0 and T_2 . The y scale has been exaggerated to allow the visualization of more sections

at the end of the crop (August 2022) (Fig. 9). There is an increase in ER in layer 1, which presents areas that are progressively resistive over time, with values that pass from 11 to 19 Ωm . These areas are linked to the growth of the root system which can reach a depth of 20 cm and to the compaction of the clay in this layer. Layer 2, on the other hand, appears to be characterized by an increase in EC over time, confirming the formation of a water accumulation zone at a depth of 40 cm with respect to the ground level.

The ERT images also highlighted a different distribution of water along the ridge, in fact by observing the sections on the surface the most conductive area is the one located in the highest portion of the ridge, i.e., in correspondence with the central line of electrodes. In correspondence with the lateral lines of electrodes, a greater EC is observed in correspondence with the line of electrodes positioned at 0.00 m compared to that positioned at 0.60 m which appears to be characterized by a greater number of areas with high resistivity. This leads to highlighting a non-homogeneous distribution of irrigation water along the ridge and consequently in depth.

Time-lapse measurements of soil EC can therefore provide useful information on the effectiveness of the irrigation system, as they allow one to observe increases in EC with the irrigation phases and thus with the increase of VWC in the soil. High-resolution ERT surveys have made it possible to identify the spatio-temporal distribution of irrigation water and thus soil moisture in the various soil layers and to identify preferential pathways of irrigation water percolation, showing an irrigation system that is not at its most efficient.

Unfortunately, the lack due to logistical issues of an ERT survey carried out prior to crop initiation, i.e., prior to planting and irrigation initiation, did not allow us to assess the change in soil moisture between the beginning and end of the crop.

The images of the EC [%] (Fig. 9) variation during and after irrigation (obtained according to Eq. 2) show a change consistent with the increase in water content. The areas highlighted in blue represent, in fact, an increase in conductivity, and therefore an increase in soil saturation. These areas represent water accumulation and by following their development from the superficial portion, where the roots are located, down to the depths, it is possible to identify the path of the irrigation water inside and below the mulch crown. This analysis leads to the identification of a particularly conductive layer at a depth between 0.00 and 0.30 cm, i.e., at the base and below the mulch peak, away from the roots.

Conclusion

ERTs conducted during the irrigation cycle of a field used for growing melons allowed to highlight the distribution of the irrigation water along the studied profile. The results show a non-homogeneous distribution of the water with respect to the two drippers position. In fact, a higher content of water infiltration emerges at electrode line 1–24 and 25–48 than at electrode line 49–72. The ERT also showed the preferential water infiltration paths along the ridge profile. Although watering holes are placed evenly along the dripline to ensure maximum uniformity and distribution of water in the root zone, the electrical topographies show the development of preferential flows which become increasingly important over time and lead to the concentration of water below the root zone (about 40 cm deep), thus making it unavailable for the roots themselves. Therefore, the employment of ERT demonstrated the poor efficiency of the two-drip-wing in this type of cultivation with mulch ridge: this system in this agricultural application is not as optimal and efficient as it should be. Further investigations are needed to test and compare, using the ERT technique, the efficiency of different irrigation systems, e.g., systems with 3 drip lines and/or different flow rates.

Results also confirm the direct correlation between EC and VWC highlighted by other authors (Vargas et al. 2021) and demonstrate the reliability of the EC as an indicator of the relative VWC variation during the irrigation cycle. Thus, EC obtained by means of a 3D ERT survey is a cost-effective and spatial indicator of the relative VWC variations. Further analyses are needed to demonstrate the reliability of this parameter also during the irrigation phase, reducing the acquisition time so that more data can be recorded in less time. Further analyses are also needed to verify the linear relationship between EC and VWC, i.e., whether it is valid for the entire study area and year by year.

The results of the 3D ERT investigations showed an unexpected result on the distribution of irrigation water within the mulch ridge, in fact the topographies showed excessive drainage below the root zone, therefore further investigations are necessary to assess the effective height of the mulch ridge so that more water remains available for the roots.

Acknowledgements The authors would like to thank O.P. Bristol Soc. Agr. Cons. a r.l. for making the research possible by conducting measurements within their field. Tommaso Concari and his collaborators, Francesco Barbadori, Antonio Pescatore, Alessio Gatto and Francesco Poggi for their support during the data collection campaign.

Author contributions Conceptualization, A.I., V.P., M.N.; methodology, A.I., V.P., M.N.; investigation, A.I., M.N.; data curation, A.I., V.P.; writing—original draft preparation, A.I., V.P.; writing—review and editing, A.I., V.P., M.N., R.F., S.O.; visualization A.I., V.P.; supervision, R.F., S.O.; project administration, R.F., S.O.; funding acquisition,

R.F., S.O. All authors have read and agreed to the published version of the manuscript.

Funding Open access funding provided by Università degli Studi di Firenze within the CRUI-CARE Agreement. No research funds have been received.

Data availability Data are available under request to the corresponding author.

Declarations

Conflict of interest The authors declare no competing interests.

Open Access This article is licensed under a Creative Commons Attribution 4.0 International License, which permits use, sharing, adaptation, distribution and reproduction in any medium or format, as long as you give appropriate credit to the original author(s) and the source, provide a link to the Creative Commons licence, and indicate if changes were made. The images or other third party material in this article are included in the article's Creative Commons licence, unless indicated otherwise in a credit line to the material. If material is not included in the article's Creative Commons licence and your intended use is not permitted by statutory regulation or exceeds the permitted use, you will need to obtain permission directly from the copyright holder. To view a copy of this licence, visit <http://creativecommons.org/licenses/by/4.0/>.

References

- Abbass K, Qasim MZ, Song H, Murshed M, Mahmood H, Younis I (2022) A review of the global climate change impacts, adaptation, and sustainable mitigation measures. *Environ Sci Pollut Res* 29(28):42539–42559
- Acosta JA, Gabarrón M, Martínez-Segura M, Martínez-Martínez S, Faz Á, Pérez-Pastor A, Gómex-López MD, Zornoza R (2022) Soil water content prediction using electrical resistivity tomography (ERT) in Mediterranean tree orchard soils. *Sensors* 22(4):1365
- Alamry AS, van der Meijde M, Noomen M, Addink EA, van Benthem R, de Jong SM (2017) Spatial and temporal monitoring of soil moisture using surface electrical resistivity tomography in Mediterranean soils. *CATENA* 157:388–396
- Allred BJ, Ehsani MR, Daniels JJ (2008) General considerations for geophysical methods applied to agriculture. *Handbook of agricultural geophysics*. CRC Press, Boca Raton, pp 3–16
- Araya Vargas J, Gil PM, Meza FJ, Yáñez G, Menanno G, García-Gutiérrez V, Luque AJ, Poblete F, Figueroa R, Maringue J, Pérez-Estay N, Sanhueza J (2021) Soil electrical resistivity monitoring as a practical tool for evaluating irrigation systems efficiency at the orchard scale: a case study in a vineyard in Central Chile. *Irrig Sci* 39:123–143
- Arora NK (2019) Impact of climate change on agriculture production and its sustainable solutions. *Environ Sustain* 2(2):95–96
- Balasco M, Lapenna V, Rizzo E, Telesca L (2022) Deep electrical resistivity tomography for geophysical investigations: the state of the art and future directions. *Geosciences* 12(12):438
- Beff L, Günther T, Vandoorne B, Couvreur V, Javaux M (2013) Three-dimensional monitoring of soil water content in a maize field using electrical resistivity tomography. *Hydrol Earth Syst Sci* 17(2):595–609
- Bellanova J, Calamita G, Catapano I, Ciucci A, Cornacchia C, Genarelli G, Giocoli A, Fisangher F, Ludeno G, Morelli G, Perrone A, Piscitelli S, Soldovieri F, Lapenna V (2020) GPR and ERT investigations in urban areas: the case-study of Matera (southern Italy). *Remote Sens* 12(11):1879
- Binley A (2015) Tools and techniques: DC electrical methods. In: Schubert G (ed) *Treatise on geophysics*. Elsevier, Cambridge, MA
- Bittelli M (2011) Measuring soil water content: a review. *HortTechnology* 21(3):293–300
- Blanchy G, Mehmandoostkotlar A, Everaert B, Huits D, Garré S, Hermans T, Nguyen F (2023) Geophysical monitoring of the fresh-saline groundwater interface in Belgian polders (No. EGU23-7736). *Copernicus Meetings*
- Blanchy G, Watts CW, Richards J, Bussell J, Huntenburg K, Sparkes DL, Stalham M, Hawkesford MJ, Whalley R, Binley A (2020) Time-lapse geophysical assessment of agricultural practices on soil moisture dynamics. *Vadose Zone J* 19(1):e20080
- Bogena HR, Huisman JA, Schilling B, Weuthen A, Vereecken H (2017) Effective calibration of low-cost soil water content sensors. *Sensors* 17(1):208
- Brindt N, Rahav M, Wallach R (2019) ERT and salinity—a method to determine whether ERT-detected preferential pathways in brackish water-irrigated soils are water-induced or an artifact of salinity. *J Hydrol* 574:35–45
- Brower C, Prins K, Heilbloem M (1989) *Irrigation water management: irrigation scheduling, training manual no. 4*. FAO, Rome
- Brunet P, Clément R, Bouvier C (2010) Monitoring soil water content and deficit using electrical resistivity tomography (ERT)—a case study in the Cevennes area. *France J Hydrol* 380(1–2):146–153
- Burt CM, Clemmens AJ, Bliesner R, Merriam JL, Hardy L (2000) Selection of irrigation methods for agriculture. *American Society of Civil Engineers*, Reston, VA
- Burton M (2010) *Irrigation management: principles and practices*. CABI, UK
- Cabrera D, Faundez C, Diaz P (2023) The use of high resolution electrical resistivity tomography (ERT) and mechanistic hydrological models to increase the efficiency of the water applied by irrigation (No. EGU23-16173). *Copernicus Meetings*
- Calamita G, Brocca L, Perrone A, Piscitelli S, Lapenna V, Melone F, Moramarco T (2012) Electrical resistivity and TDR methods for soil moisture estimation in central Italy test-sites. *J Hydrol* 454–455:101–112. <https://doi.org/10.1016/j.jhydrol.2012.06.001>
- Callaghan MV, Head FA, Cey EE, Bentley LR (2017) Salt leaching in fine-grained, macroporous soil: negative effects of excessive matrix saturation. *Agric Water Manag* 181:73–84
- Capello MA, Shaughnessy A, Caslin E (2021) The geophysical sustainability atlas: mapping geophysics to the UN sustainable development goals. *Lead Edge* 40(1):10–24
- Cassiani G, Boaga J, Vanella D, Perri MT, Consoli S (2015) Monitoring and modelling of soil–plant interactions: the joint use of ERT, sap flow and eddy covariance data to characterize the volume of an orange tree root zone. *Hydrol Earth Syst Sci* 19(5):2213–2225
- Catelani M, Ciani L, Guidi G, Patrizi G, Casagli N, Ceccatelli M, Pazzi V, Cappuccini L (2021) Effects of inaccurate electrode positioning in subsurface resistivity measurements for archaeological purposes. In: 2021 IEEE international instrumentation and measurement technology conference (I2MTC). IEEE, pp 1–6
- Cogato A, Meggio F, De Antoni Migliorati M, Marinello F (2019) Extreme weather events in agriculture: a systematic review. *Sustainability* 11(9):2547
- Corwin DL, Lesch SM (2014) A simplified regional-scale electromagnetic induction—salinity calibration model using ANOCOVA modeling techniques. *Geoderma* 230:288–295
- Dahlin T, Zhou B (2004) A numerical comparison of 2D resistivity imaging with 10 electrode arrays. *Geophys Prospect* 52(5):379–398

- De Carlo L, Battilani A, Solimando D, Caputo MC (2020) Application of time-lapse ERT to determine the impact of using brackish wastewater for maize irrigation. *J Hydrol* 582:124465
- Dezert T, Fargier Y, Lopes SP, Cote P (2019) Geophysical and geotechnical methods for fluvial levee investigation: a review. *Eng Geol* 260:105206
- Di Maio R, De Paola C, Forte G, Piegari E, Pirone M, Santo A, Urcioli G (2020) An integrated geological, geotechnical and geophysical approach to identify predisposing factors for flowslide occurrence. *Eng Geol* 267:105473
- Garré S, Hyndman D, Mary B, Werban U (2021) Geophysics conquering new territories: the rise of “agrogeophysics.” *Vadose Zone J* 20(4):e20115
- Garré S, Javaux M, Vanderborght J, Pagès L, Vereecken H (2011) Three-dimensional electrical resistivity tomography to monitor root zone water dynamics. *Vadose Zone J* 10(1):412–424
- Hannian SE, Hijab BR, Laftah AA (2021) Geophysical investigation of Babylon archeological City, Iraq. *Diyala J Pure Sci* 17(03)
- Hayley K, Bentley LR, Gharibi M, Nightingale M (2007) Low temperature dependence of electrical resistivity: implications for near surface geophysical monitoring. *Geophys Res Lett* 34(18)
- Heaney MB (2003) Electrical conductivity and resistivity. In: Webster J (ed) *Electrical measurement, signal processing, and displays*. CRC Press, pp 1–14
- Howell TA (2003) Irrigation efficiency. *Encycl Water Sci* 467:500
- Hussain Y, Schlögel R, Innocenti A, Hamza O, Iannucci R, Martino S, Havenith HB (2022) Review on the geophysical and UAV-based methods applied to landslides. *Remote Sens* 14(18):4564
- Innocenti A, Pazzi V, Napoli M, Fanti R, Orlandini S (2022) Application of electrical resistivity tomography (ERT) to study soil water and salt movement under drip irrigation in a saline soil cultivated with melon. In: *EGU general assembly conference abstracts*, pp EGU22-4469
- Innocenti A, Rosi A, Tofani V, Pazzi V, Gargini E, Masi EB, Segoni S, Bertolo D, Paganone M, Casagli N (2023) Geophysical surveys for geotechnical model reconstruction and slope stability modelling. *Remote Sens* 15(8):2159
- Israelsen OW (1950) *Irrigation principles and practices*, vol 471. Wiley, New York
- Jensen ME (2007) Beyond irrigation efficiency. *Irrig Sci* 25(3):233–245
- Jodry C, Lopes SP, Fargier Y, Sanchez M, Côte P (2019) 2D-ERT monitoring of soil moisture seasonal behaviour in a river levee: a case study. *J Appl Geophys* 167:140–151
- Loke MH (2014) Tutorial: 2-D and 3-D electrical imaging surveys. https://web.gps.caltech.edu/classes/ge111/Docs/ResNotes_Loke.pdf
- Ma D, Doussan C, Chapelet A, Charron F, Olioso A (2011) Monitoring soil to groundwater preferential flow during border irrigation using time-lapse ERT. In: *Geophysical research abstracts*, Vol. 13
- Malhi GS, Kaur M, Kaushik P (2021) Impact of climate change on agriculture and its mitigation strategies: a review. *Sustainability* 13(3):1318
- Mary B, Vanella D, Consoli S, Cassiani G (2019) Assessing the extent of citrus trees root apparatus under deficit irrigation via multi-method geo-electrical imaging. *Sci Rep* 9(1):9913
- Nijland W, Van der Meijde M, Addink EA, De Jong SM (2010) Detection of soil moisture and vegetation water abstraction in a Mediterranean natural area using electrical resistivity tomography. *CATENA* 81(3):209–216
- Ortega-Reig M, Sanchis-Ibor C, Palau-Salvador G, García-Mollá M, Avellá-Reus L (2017) Institutional and management implications of drip irrigation introduction in collective irrigation systems in Spain. *Agric Water Manag* 187:164–172
- Patrizi G, Guidi G, Ciani L, Catelani M, Cappuccini L, Innocenti A, Casagli N, Pazzi V (2022). Analysis of non-ideal remote pole in electrical resistivity tomography for subsurface surveys. In: 2022 IEEE international instrumentation and measurement technology conference (I2MTC). IEEE, pp 1–5
- Pazzi V, Ciani L, Cappuccini L, Ceccatelli M, Patrizi G, Guidi G, Casagli N, Catelani M (2019a) ERT investigation of tumuli: does the errors in locating electrodes influence the resistivity. In: *Proceedings of the IMECO TC-4 international conference on metrology for archaeology and cultural heritage*, Florence, Italy, pp 4–6
- Pazzi V, Di Filippo M, Di Nezza M, Carlà T, Bardi F, Marini F, Fontanelli K, Intrieri E, Fanti R (2018) Integrated geophysical survey in a sinkhole-prone area: microgravity, electrical resistivity tomographies, and seismic noise measurements to delimit its extension. *Eng Geol* 243:282–293
- Pazzi V, Morelli S, Fanti R (2019b) A review of the advantages and limitations of geophysical investigations in landslide studies. *Int J Geophys* 2019:1–27
- Perrone A, Lapenna V, Piscitelli S (2014) Electrical resistivity tomography technique for landslide investigation: a review. *Earth Sci Rev* 135:65–82
- Ronchi D, Limongiello M, Demetrescu E, Ferdani D (2023) Multi-spectral UAV data and GPR survey for archeological anomaly detection supporting 3D reconstruction. *Sensors* 23(5):2769
- Santarato G, Ranieri G, Occhi M, Morelli G, Fischanger F, Gualerzi D (2011) Three-dimensional electrical resistivity tomography to control the injection of expanding resins for the treatment and stabilization of foundation soils. *Eng Geol* 119(1–2):18–30
- Sendrós A, Himi M, Lovera R, Rivero L, Garcia-Artigas R, Urruela A, Casas A (2020) Geophysical characterization of hydraulic properties around a managed aquifer recharge system over the Llobregat River Alluvial Aquifer (Barcelona Metropolitan Area). *Water* 12(12):3455
- Slepek Z, Platov B (2019) Geophysics in archeology. In: *Practical and theoretical aspects of geological interpretation of gravitational, magnetic and electric fields: proceedings of the 45th Uspensky international geophysical seminar*, Kazan, Russia. Springer International Publishing, pp 303–311
- Van der Kooij S, Zwarteveen M, Boesveld H, Kuper M (2013) The efficiency of drip irrigation unpacked. *Agric Water Manag* 123:103–110
- Vanella D, Cassiani G, Busato L, Boaga J, Barbagallo S, Binley A, Consoli S (2018) Use of small scale electrical resistivity tomography to identify soil-root interactions during deficit irrigation. *J Hydrol* 556:310–324
- Vanella D, Peddinti SR, Kisekka I (2022) Unravelling soil water dynamics in almond orchards characterized by soil-heterogeneity using electrical resistivity tomography. *Agric Water Manag* 269:107652
- Viero A, Galgaro A, Morelli G, Breda A, Francese RG (2015) Investigations on the structural setting of a landslide-prone slope by means of three-dimensional electrical resistivity tomography. *Nat Hazards* 78:1369–1385
- Yu L, Gao W, Shamshiri R, Tao S, Ren Y, Zhang Y, Su G (2021) Review of research progress on soil moisture sensor technology. *Int J Agric Biol Eng* 14:32–42